Theory of solid-state harmonic generation governed by crystal symmetry

Chen Qian,[1,2] Shicheng Jiang,[3] Tong Wu,[1] Hongming Weng,[2,4,5,*] Chao Yu,[1,†] and Ruifeng Lu[1,‡]

[1]*Institute of Ultrafast Optical Physics, MIIT Key Laboratory of Semiconductor Microstructure and Quantum Sensing, Department of Applied Physics, Nanjing University of Science and Technology, Nanjing 210094, People's Republic of China*

[2]*Institute of Physics, Chinese Academy of Sciences, Beijing National Laboratory for Condensed Matter Physics, Beijing 100190, People's Republic of China*

[3]*State Key Laboratory of Precision Spectroscopy, East China Normal University, Shanghai 200062, China*

[4]*School of Physics, University of Chinese Academy of Sciences, Beijing 100049, China*

[5]*Songshan Lake Materials Laboratory, Dongguan, Guangdong 523808, China*

(Received 11 January 2024; revised 17 March 2024; accepted 8 April 2024; published 2 May 2024)

The solid-state harmonic generation (SSHG) derives from photocurrent coherence. The crystal symmetry, including point-group symmetry and time-reversal symmetry, constrains the amplitude and phase of the photocurrent, thus manipulates the coherent processes in SSHG. We revisit the expression of photocurrent under the electric dipole approximation and give an unambiguous picture of nonequilibrium dynamics of photocarriers on laser-dressed effective bands. In addition to the dynamical phase, we reveal the indispensable roles of the phase difference of transition dipole moments and the phase induced by shift vector in the photocurrent coherence. The microscopic mechanism of the selection rule, orientation dependence, polarization characteristics, time-frequency feature, and ellipticity dependence of harmonics governed by symmetries is uniformly clarified in our theoretical framework. Finally, we propose a nonlinear optical method for detecting the time-reversal symmetry breaking of crystals by using elliptical dichroism of SSHG. This work integrates nonequilibrium electronic dynamics of condensed matter in strong laser fields, and paves a way to explore more nonlinear optical phenomena governed by crystal symmetry.

DOI: 10.1103/PhysRevB.109.205401

I. INTRODUCTION

The nonlinear photocurrent in a crystal driven by strong laser fields can coherently emit solid-state harmonic generation (SSHG) [1,2]. Since the dynamical process of accelerated carrier is very sensitive to intrinsic properties of materials, SSHG has the capability of detecting the band structure [3–5], topological geometries [6–14], and strongly correlated interaction [15–18]. Each of these relates to the knowledge of crystal symmetry. The space-time symmetry of the applied field combined with the crystal symmetry provides strict coherence conditions for photocurrent, which can be recorded by harmonic signal that conforms to the selection rules [19–24]. In the last decade, the correspondence between crystal symmetry and SSHG has been confirmed adequately in literatures. However, a complete microscopic framework for illuminating the photocurrent coherence in solids has not yet been established.

In the absence of external fields, the symmetry of band structures and wave functions is prescribed by the crystal symmetry. With the addition of ultrafast oscillating laser fields, a handful of electrons are excited into the conduction band and form paired electric dipoles with holes in the valence band. The dipoles are forced to oscillate in the electric potential formed by the Coulomb and laser fields, coherently producing harmonic radiation. Much intrinsic information about crystal bands can be traced by these moving dipoles.

The roles of the band structure [25], Berry curvature [7], transition dipole moment [26], and shift vector [14] have been successively reported to reveal the dynamical process of photoelectrons. These theoretical explorations are consistent with the experimental results. Even-order harmonics in the vertical polarization can be induced by the Berry curvature, group velocity, or interband transition as previously reported [7,25,26]. However, the Berry curvature comes from first-order correction in the electron transition approximated by the perturbation theory, and its contribution can be attributed to the interband transition process when nonperturbative transition dominates [6,27]. Therefore, the origin of harmonics should be reviewed based on the behavior of electron transitions. In addition, the theoretical analysis proposed by Vampa *et al.* in 2014 shows that the phase of photocurrent only contains the dynamical phase [28]. Moreover, Jiang *et al.* emphasize the indispensability of the transition dipole phase (TDP) that it is unreasonable to artificially remove it during numerical calculations [26,29]. Later, Li *et al.* and Yue *et al.* confirm that the Berry connection should also be considered to ensure the gauge invariance of the photocurrent [30,31]. Remarkably, Wilhelm *et al.* analytically rederive the semiconductor Bloch equations under the Bloch basis, and apply the formalism to Dirac metal [32]. In recent years, the

*hmweng@iphy.ac.cn
†chaoyu@njust.edu.cn
‡rflu@njust.edu.cn

numerical method for calculating time-dependent photocurrent using density matrix equations has been improved, which is qualitatively consistent with experiments [33–37]. Nevertheless, the microscopic interference process of photocurrent involved has not been clarified. In particular, the effects of shift vector and TDP are poorly understood in strong-field physics.

In this paper, we derive the selection rule of SSHG via analytic expressions of photocurrent and reveal the role of TDP difference in the photocurrent coherence. We are committed to clarifying the symmetry dependence of SSHG with a fundamental picture involving the TDP difference and shift vector. In particular, we will use our theoretical framework to discuss the orientation dependence, polarization property, time-frequency analysis, and ellipticity dependence of harmonics determined by crystal symmetry.

II. THEORY

Considering the rationality of single-electron and dipole approximations in appropriate strong-field environment, we derive expressions of interband and intraband currents through two-band semiconductor Bloch equations as follows [28,30,32] (see Appendix A for details, atomic units are used throughout unless otherwise stated):

$$\mathbf{J}^a_{nm}(t) = -\frac{1}{N_c}\sum_{\mathbf{K}\in \mathrm{BZ}}\int_{-\infty}^{t} dt' \varepsilon_{nm}[\mathbf{k}(t)]|\mathbf{d}^a_{nm}[\mathbf{k}(t)]|\left[\mathbf{E}^b(t')\cdot\left|\mathbf{d}^b_{mn}\left[\mathbf{k}(t')\right]\right|\right] f_{nm}(\mathbf{K},t) e^{-i\left[S_{\mathrm{dyn}}(\mathbf{K},t,t')+S_{\mathrm{shift}}(\mathbf{K},t,t')+S_{\Delta\mathrm{TDP}}[\mathbf{k}(t)]\right]}, \tag{1}$$

$$\mathbf{J}^a_{nn}(t) = \frac{1}{N_c}\sum_{\mathbf{K}\in \mathrm{BZ}}\int_{-\infty}^{t} dt' \int_{-\infty}^{t'} dt'' \partial_{\mathbf{k}_a}\varepsilon_n[\mathbf{k}(t)]\left[\mathbf{E}^b(t')\cdot\left|\mathbf{d}^b_{nm}\left[\mathbf{k}(t')\right]\right|\right]\left[\mathbf{E}^b(t'')\cdot\left|\mathbf{d}^b_{mn}\left[\mathbf{k}(t'')\right]\right|\right] f_{nm}(\mathbf{K},t')$$
$$\times e^{-i\left\{S_{\mathrm{dyn}}(\mathbf{K},t',t'')+S_{\mathrm{shift}}(\mathbf{K},t',t'')+S_{\Delta\mathrm{TDP}}[\mathbf{k}(t')]\right\}} + \mathrm{c.c.}, \tag{2}$$

where a and b are Cartesian indices, labeling the directions of the currents $\mathbf{J}(t)$ and the electric field $\mathbf{E}(t)$, respectively. N_c is the total number of unit cells. Houston basis is used here. The quasimomentum $\mathbf{k}(t)$ of electrons changes adiabatically with the laser field, and the evolution relationship is $\mathbf{k}(t) = \mathbf{K} + \mathbf{A}(t)$. $\mathbf{K}$ is the canonical momentum of the crystal in the absence of field. Here, the transition dipole matrix element $\mathbf{d}_{nm}(\mathbf{k}) = i\langle u_{n,\mathbf{k}}|\partial_{\mathbf{k}}|u_{m,\mathbf{k}}\rangle$ describes the polarization of electron-hole pairs. $f_{nm}(\mathbf{K},t) = \rho_{nn}(\mathbf{K},t) - \rho_{mm}(\mathbf{K},t)$ is the difference of Fermi-Dirac distribution, and the band index $n \neq m$.

There are three phase factors that determine the photocurrent coherence. First, the dynamical phase

$$S_{\mathrm{dyn}}(\mathbf{K},t,t') = \int_{t'}^{t} \varepsilon_{mn}[\mathbf{k}(\tau)]d\tau, \tag{3}$$

where $\varepsilon_{mn}(\mathbf{k}) = \varepsilon_m(\mathbf{k}) - \varepsilon_n(\mathbf{k})$ is the energy difference between bands n and m.

Second, a shift phase is introduced as

$$S_{\mathrm{shift}}(\mathbf{K},t,t') = \int_{t'}^{t} \mathbf{E}^b(\tau)\cdot\mathbf{R}^{b,b}_{mn}[\mathbf{k}(\tau)]d\tau, \tag{4}$$

where the shift vector $\mathbf{R}^{b,b}_{mn}(\mathbf{k}) = \mathbf{d}^b_{mm}(\mathbf{k}) - \mathbf{d}^b_{nn}(\mathbf{k}) - \partial_{\mathbf{k}_b}\phi^b_{mn}(\mathbf{k})$, formed by the Berry connections and TDP, represents the offset of charge centers of different bands [14,38]. $\phi^a_{mn}(\mathbf{k})$ is the TDP as $\mathbf{d}^a_{mn}(\mathbf{k}) = |\mathbf{d}^a_{mn}(\mathbf{k})|e^{i\phi^a_{mn}(\mathbf{k})}$. $|\mathbf{d}^a_{mn}(\mathbf{k})|$ is the transition dipole amplitude and denotes the polarization intensity of electron-hole pair.

The third phase factor

$$S_{\Delta\mathrm{TDP}}(\mathbf{k}) = \phi^a_{mn}(\mathbf{k}) - \phi^b_{mn}(\mathbf{k}) \tag{5}$$

denotes the difference of transition dipole phases (ΔTDP) along a and b directions, which comes from the deflection of noncollinear currents relative to the driving field.

Each of the three phase factors is gauge independent. The total current is $\mathbf{J}^a = \sum_{n,m}(\mathbf{J}^a_{nm} + \mathbf{J}^a_{nn})$. From Eqs. (1) and (2), we notice that the phases of interband and intraband currents have the same form; thus, the symmetry dependence of their coherence in laser-crystal systems is always consistent.

A. ΔTDP-determined selection rules of SSHG

One of the most widely studied and robust laws in SSHG is its selection rule, which mainly depends on the crystal symmetry and can be divided into two categories. The first type appears in the typical Floquet systems and results from periodic oscillations of laser fields. Photoexcited carriers can display dynamical symmetry and coherently generate harmonic radiation [22]. The other is induced directly by the crystal symmetry that is not broken by applied fields. The photocurrents cancel each other out, leading to no harmonic in some particular directions.

In the strong-laser regime, external electric field can be compared with the Coulomb field in crystals, it cannot be regarded as a perturbation. In this case, we need to consider the influence of the time-dependent population of charge density on the nonlinear process. Therefore, compared with the perturbation approximation, a broader theory is expected to treat systems under strong laser fields.

The crystal symmetry we considered here includes the point-group symmetry and time-reversal symmetry. Due to the periodic translational symmetry, crystals are limited to 32 point groups and 122 magnetic point groups. In addition, the laser fields could also contain abundant time-space symmetry. By combining the symmetries of crystals and light fields, we can obtain a wide variety of selection rules for SSHG. In this paper, we further explore more fundamental microscopic dynamics underlying these rules.

Consider a point-group symmetry operation $\hat{G}$ on the transition dipole matrix element (see Appendix B for derivations), we have

$$\hat{G}\mathbf{d}^a_{nm}(\mathbf{k})\hat{G}^\dagger = \mathbf{d}^{a'}_{nm}(G^{-1}\mathbf{k}) = G_{a'a}\mathbf{d}^a_{nm}(\mathbf{k}), \tag{6}$$

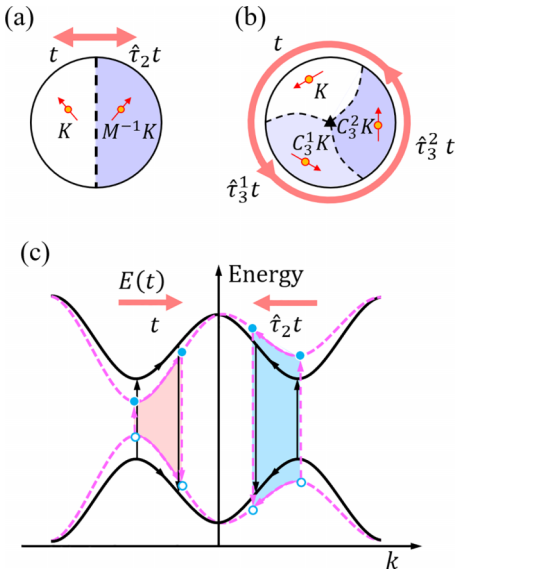

FIG. 1. Diagrams of dipole interference induced by dynamical symmetries. (a) Mirror symmetry combined with order-2 temporal symmetry of light. (b) Threefold rotational symmetry combined with order-3 temporal symmetry of light. The red arrows represent the polarization of laser field. The dipoles excited in different subcycles are indicated by dotted arrows, which are linked by corresponding symmetry operations, respectively. (c) Interference pattern of two channels in reciprocal space. The solid black lines are symmetric bands and channels protected by the inversion symmetry. The magenta dashed line is the effective bands deformed by the laser field, its asymmetry comes from the inversion symmetry breaking of crystals. The arrows between the bands indicate electronic excitation and electron-hole recombination, while the arrows along the band dispersions show acceleration of electron-hole pair. Different color areas surrounded by the arrows highlight the asymmetry of the channels.

in which $a, a' = G^{-1}a$ denote the directions of the transition dipole moments, $G_{a'a} = e^{i[\phi^{a'}_{nm}[\mathbf{k}(t)]-\phi^{a}_{nm}[\mathbf{k}(t)]]}$ is just the ΔTDP between a and a' direction under $\hat{G}$. Moreover, the scalar quantities such as the dynamical phase and shift phase are invariant under $\hat{G}$.

With the addition of the light field, let us combine $\hat{G}$ and order-N time translation operator ($N \in \mathbb{N}$, $\mathbb{N}$ denotes set of natural numbers):

$$\hat{X} = \hat{G} \cdot \hat{\tau}_N \tag{7}$$

with $\hat{\tau}_N t \equiv t \pm \frac{T_0}{N}$, $T_0 = \frac{2\pi}{\omega_0}$ is the period of the laser field of frequency ω_0. We apply the dynamical symmetry operation to the photocurrent,

$$\hat{X}\mathbf{J}^a(\mathbf{K}, t)\hat{X}^\dagger = \mathbf{J}^{G^{-1}a}(G^{-1}\mathbf{K}, \hat{\tau}_N t). \tag{8}$$

Every wave vector $\mathbf{K}$ in the lattice is a candidate for harmonic peaks unless symmetry forbids it. For the time-dependent quasimomentum $\mathbf{k}(t) \equiv \mathbf{K} + \mathbf{A}(t)$,

$$\hat{X}\mathbf{k}(t) = G^{-1}\mathbf{K} + \mathbf{A}(\hat{\tau}_N t). \tag{9}$$

The action of the laser field may disrupt initial symmetries of crystals, but new dynamical symmetry can be induced. Based on the above transformation rules, we can derive that the interband current with dynamical symmetry can transform as

$$\begin{aligned}\hat{X}\mathbf{J}^a_{nm}(\mathbf{K}, t)\hat{X}^\dagger &= \mathbf{J}^{G^{-1}a}_{nm}(G^{-1}\mathbf{K}, \hat{\tau}_N t) \\ &= -i\varepsilon_{nm}[\mathbf{k}(t)]G_{a'a}\mathbf{d}^a_{nm}[\mathbf{k}(t)]\rho_{nm}(\mathbf{K}, t) \\ &= \mathbf{J}^a_{nm}(\mathbf{K}, t)e^{iS_{\Delta\mathrm{TDP}}(\mathbf{k}(t))}.\end{aligned} \tag{10}$$

The electron density ρ_{nm} is approximatively invarible under the dynamical symmetry operation. The same transformation rule is followed for the intraband counterpart.

We find that all the point-group dynamical symmetry operations only induce a change of photocurrent phase, which is the ΔTDP. That is, the transformation occurs only at the argument or the phase of the transition dipole, but the band dispersion, transition dipole amplitude, dynamical phase, and shift phase are invariant. The coherence of harmonics stems from the interference between transition dipoles with different arguments associated by the dynamic symmetry [Figs. 1(a) and 1(b) show schematics of coherent dipoles under the mirror symmetry and rotational symmetry, respectively]. Equation (10) is universal and can be applied to all selection rules arising from point-group symmetry. More detailed derivation for typical cases of basic symmetry operations can be found in Appendix C. In Tables I and II, ΔTDP-determined selection rules of SSHG are shown for the mirror symmetry and rotational symmetry.

TABLE I. Selection rule of SSHG by mirror symmetry. a and b represent directions of photocurrent and laser field, respectively, and c is the normal direction of crystal mirror plane. $l \in \mathbb{N}$.

	$a \parallel c$	$a \perp c$
$b \parallel c$	$\Delta\mathrm{TDP} = \pi, \omega = (2l+1)\omega_0$	$\Delta\mathrm{TDP} = 0, \omega = 2l\omega_0$
$b \perp c$	No harmonics	Integer order harmonics

B. Role of shift phase in three-step model of SSHG

The role of shift phase induced by applied electric barriers in SSHG has not been clarified so far. To demonstrate the indispensable role of shift phase in the process of photocurrent coherence, we compare order-2 dynamical coherence processes formed by spatial-inversion symmetry with time-reversal symmetry.

The second harmonic generation is one of the most common methods to determine the inversion symmetry of crystals. We know that when we apply a monochromatic light to a centrosymmetric crystal, even-order harmonics can be canceled by destructive interference, while the odd-order harmonics show constructive interference.

TABLE II. Selection rule of SSHG by rotational symmetry. c is the direction of crystal rotational axis, and the other parameters are the same as Table I.

	$a \perp c$	$a \parallel c$
$b \perp c$	$\Delta\mathrm{TDP} = \pm\frac{2\pi}{N}, \omega = (Nl \pm 1)\omega_0$	$\Delta\mathrm{TDP} = 0, \omega = Nl\omega_0$
$b \parallel c$	No harmonics	Integer order harmonics

Let $\hat{P} = \hat{I} \cdot \hat{\tau}_2$, $\hat{I}$ is the spatial-inversion operation. Using Eq. (10), the interband current under $\hat{P}$ transforms as

$$\hat{P}\mathbf{J}^a_{nm}(\mathbf{K}, t)\hat{P}^\dagger = \mathbf{J}^{I^{-1}a}_{nm}(-\mathbf{K}, \hat{\tau}_2 t) = -\mathbf{J}^a_{nm}(\mathbf{K}, t). \tag{11}$$

Integrating over the entire BZ, we then have $\mathbf{J}^{I^{-1}a}_{nm}(\hat{\tau}_2 t) = -\mathbf{J}^a_{nm}(t)$. The reversal of the current comes from the inversed dipole moment. After applying Fourier transform, we know that the radiated photon frequency is $\omega = (2l+1)\omega_0, l \in \mathbb{N}$. The same conclusion can be reached by analyzing the intraband current.

Similarly, we define an operator $\hat{U}$ that performs time-reversal operation $\hat{T}$ on the crystals and order-2 temporal operator $\hat{\tau}_2$ on the time. The time-dependent quasimomentum has $\hat{U}\mathbf{k}(t) = -\mathbf{k}(t)$. The interband current under $\hat{U}$ takes (see Appendix D for details)

$$\begin{aligned}\hat{U}\mathbf{J}^a_{nm}(\mathbf{K}, t)\hat{U}^\dagger &= \mathbf{J}^a_{nm}(-\mathbf{K}, \hat{\tau}_2 t) \\ &= -\mathbf{J}^a_{nm}(\mathbf{K}, t)e^{2i[S_{\text{shift}}(\mathbf{K},t,t')+S_{\Delta\text{TDP}}[\mathbf{k}(t)]]}.\end{aligned} \tag{12}$$

By comparing Eqs. (11) and (12), it can be found that the impact of $\hat{P}$ and $\hat{U}$ on the photocurrent differs by the shift phase and ΔTDP. The shift phase vanishes in crystals with both time-reversal symmetry and inversion symmetry (see Appendix D for derivations). However, by time-reversal symmetry alone, a phase mismatch between the dynamical phase and shift phase as well as between dynamical phase and ΔTDP will be caused, and completely destructive interference cannot be formed. Since the inversion symmetry results in pure odd-order harmonic generation, the shift phase and ΔTDP should be crucial factors for even-order harmonic generation in crystals with time-reversal symmetry.

A channel of the three-step model in strong-field physics includes excitation, acceleration, and recollision processes of an electron-hole pair. Let us further consider two interference channels driven by monochromatic laser field as Fig. 1(c) shows. When inversion symmetry exists, the two channels are identical with an interval of half an optical cycle (black arrows indicate), their interference leads to pure odd-order harmonics. If the system only possesses time-reversal symmetry, then these two channels are going to be different (magenta arrows indicate). The band dispersion and transition dipole amplitude remain symmetric in k space due to the protection of time-reversal symmetry. However, due to the existence of the shift vector in noncentrosymmetric crystals, electrons need to do extra work in the photoelectric field when they take interband transitions [14]. Thus, the external light field equivalently modulates the energy curve of electrons like Coulomb field, and forming the laser-dressed effective bands with symmetry breaking in k space [magenta dashed curves in Fig. 1(c)]. Therefore, extra shift phase accumulates in addition to the dynamical phase when pairs of dipoles perform intraband motions. The interference condition of pure odd-order harmonics is broken and even-order harmonics can be produced. The movement of electron-hole pairs on the effective bands simultaneously accumulates the dynamical phase and shift phase, which have fully equivalent effects on the photocurrent and together constitute its phase:

$$S_{\text{J}}(\mathbf{K}, t, t') = S_{\text{dyn}}(\mathbf{K}, t, t') + S_{\text{shift}}(\mathbf{K}, t, t') + S_{\Delta\text{TDP}}[\mathbf{k}(t)]. \tag{13}$$

This fundamental image of interference involving two channels can be easily generalized to multiple channels. Therefore, the coherence process of SSHG can be clearly described by coherent channels of dipoles on the laser-dressed effective bands.

C. Using circular dichroism to discriminate time-reversal symmetry breaking

Based on above discussions, we continue to search for rules of SSHG that could be caused by time-reversal symmetry. The inversion symmetry breaking of crystals can be judged by even-order harmonic generation, which arises from interference of nonequivalent currents between two adjacent half-cycles. Similarly, we can utilize laser fields with opposite helicities to find evidence of time-reversal symmetry breaking. The helicity of elliptically polarized light can be flipped by $\hat{T}$ without considering the Poynting vector of lights. It is found that the transport processes of charge carriers are different in magnetic materials driven by lasers with different helicity. In experiments, the magnetic circular dichroism of nonlinear optical response has been used to record the magnetic switching of materials [39–42]. The circular dichroism caused by laser fields also have access to selective excitation of spin, valley, and chirality of electron states [43–46].

In the following, we will demonstrate that the circular dichroism of SSHG is directly related to the time-reversal symmetry breaking of crystal by our theoretical method. Under the time-reversal transformation, the initial right-hand helically polarized laser (σ_+) is changed to left-hand helically polarized laser (σ_-), which have $\mathbf{E}_{\sigma_+}(t) = \mathbf{E}_{\sigma_-}(-t)$, and $\mathbf{A}_{\sigma_+}(t) = -\mathbf{A}_{\sigma_-}(-t)$. Each component of the photocurrent phase has the following transformation relation:

$$\begin{aligned}\hat{T}S_{\text{dyn}}(\mathbf{K}, \mathbf{A}_{\sigma_+}, t, t')\hat{T}^\dagger &= S_{\text{dyn}}(-\mathbf{K}, \mathbf{A}_{\sigma_-}, -t, -t') \\ &= -S_{\text{dyn}}(\mathbf{K}, \mathbf{A}_{\sigma_+}, t, t'),\end{aligned} \tag{14}$$

$$\begin{aligned}\hat{T}S_{\text{shift}}(\mathbf{K}, \mathbf{A}_{\sigma_+}, t, t')\hat{T}^\dagger &= S_{\text{shift}}(-\mathbf{K}, \mathbf{A}_{\sigma_-}, -t, -t') \\ &= -S_{\text{shift}}(\mathbf{K}, \mathbf{A}_{\sigma_+}, t, t'),\end{aligned} \tag{15}$$

$$\begin{aligned}\hat{T}S_{\Delta\text{TDP}}(\mathbf{K} + \mathbf{A}_{\sigma_+}(t))\hat{T}^\dagger &= S_{\Delta\text{TDP}}(-\mathbf{K} + \mathbf{A}_{\sigma_-}(-t)) \\ &= -S_{\Delta\text{TDP}}(\mathbf{K} + \mathbf{A}_{\sigma_+}(t)).\end{aligned} \tag{16}$$

The dynamical phase, shift phase, and ΔTDP all reverse signs under $\hat{T}$, but this cannot be achieved by any pure point-group symmetry. Accordingly, the interband current generated by helically polarized lasers transforms as (see Appendix D for derivations)

$$\begin{aligned}\hat{T}\mathbf{J}^a_{nm,\sigma_+}(\mathbf{K}, t)\hat{T}^\dagger &= \mathbf{J}^a_{nm,\sigma_-}(-\mathbf{K}, -t) \\ &= -\mathbf{J}^{a,*}_{nm,\sigma_+}(\mathbf{K}, t)\frac{f_{nm}(-\mathbf{K}, -t)}{f_{nm}(\mathbf{K}, t)}.\end{aligned} \tag{17}$$

If we assume that the difference of Fermi-Dirac distribution is time-reversal invariant [i.e., $f_{nm}(-\mathbf{K}, -t) = f_{nm}(\mathbf{K}, t)$], the interband current has $\hat{T}\mathbf{J}^a_{nm,\sigma_+}(t)\hat{T}^\dagger = -\mathbf{J}^{a,*}_{nm,\sigma_+}(t)$. This assumption can work in the perturbation regime with low-order changing rate of electron distribution. For the intraband current, the same conclusion can be derived. Then we have $\hat{T}\mathbf{J}^a_{\sigma_+}(t)\hat{T}^\dagger = \mathbf{J}^a_{\sigma_-}(-t) = -\mathbf{J}^a_{\sigma_+}(t)$, so lasers with opposite

helicity can produce SSHG with the same intensity. We deduce that, under the protection of the time-reversal symmetry of crystals, the intensity of low-order nonlinear optical response does not show the circular dichroism. In contrast, the circular dichroism emerges when magnetic materials are considered. It allows us to use helically polarized laser fields to detect the magnetism of crystals. Later, we will show a deeper discussion into the validity and limitations of harmonic circular dichroism (or elliptical dichroism).

III. MODEL CALCULATION

We have theoretically revealed the role of the ΔTDP and the shift phase in symmetric rules of SSHG. Now we perform numerical calculations based on tight-binding models including the graphene, h-BN, and Haldane model [47] to justify our theoretical insight.

A. Orientation dependence and polarization characteristics

Our discussion focuses on tight-binding models with honeycomb lattice due to its universality. Considering the hopping to the nearest-neighbor sites, the Hamiltonian is

$$H = t_1 \sum_{\langle i,j \rangle} c_i^\dagger c_j, \tag{18}$$

where i, j denote different sublattices. This is the simplest two-band Hamiltonian used to describe the graphene, which is subject to D_{6h} point-group and time-reversal symmetries. For calculations, we set the lattice constant to 2.5 Å and the nearest-neighbor hopping t_1 to 2.33 eV. The peak intensity of the driving laser we selected is 1.2×10^{12} W/cm^2, wavelength is 1.9 μm, and full width at half-maximum is 55 fs in a Gaussian envelope.

Figure 2 shows the polarization characteristics of harmonics parallel and perpendicular to linearly polarized laser field as a function of crystal orientation. The orientation angle θ is set to 0° when the laser is along Γ-K direction. Pure odd-order harmonics are generated due to the inversion symmetry of graphene [see Figs. 2(a) and 2(b)]. The C_6 axis out of plane leads to the orientation periodicity of 60° for all harmonics.

Let us break the inversion symmetry by introducing different onsite energy for adjacent atoms, the Hamiltonian is

$$H = t_1 \sum_{\langle i,j \rangle} c_i^\dagger c_j + M_0 \sum_i \epsilon_i c_i^\dagger c_i, \tag{19}$$

in which $\epsilon_i = \pm 1$ for different atoms. It can be used to describe hexagonal boron nitride (h-BN), its point-group symmetry is reduced to D_{3h}. Different from the graphene, even harmonics are generated due to the inversion symmetry breaking [see Figs. 2(c) and 2(d)]. The inversion symmetry-breaking term M_0 is set to 1.96 eV. The interference processes in time domain can be reflected by time-frequency analysis spectra. Combining Figs. 3(b) and 3(d), we now know that even-order harmonics results from the difference of harmonic radiations between adjacent half-cycles. By analyzing Eq. (13), the inverted laser field every half optical cycle cannot change the dynamical phase. However, the shift phase as well as ΔTDP formed by the two unequal interference channels are different, which are responsible for the different temporal harmonic radiations and even-order harmonic generation in noncentrosymmetric crystals. We plot time-dependent effective potential under the laser modification, calculated by $\varepsilon_{mn}[\mathbf{k}(t)] + \mathbf{E}(t) \cdot \mathbf{R}_{mn}[\mathbf{k}(t)]$. The photocurrent phase is the integral of the effective potential in time domain [see channels 1 and 2 in Figs. 3(c) and 3(e), which are the same for graphene but different for h-BN]. In Fig. 3, only the parallel component of photocurents is considered, thus, the ΔTDP vanish here but exist for other polarization directions.

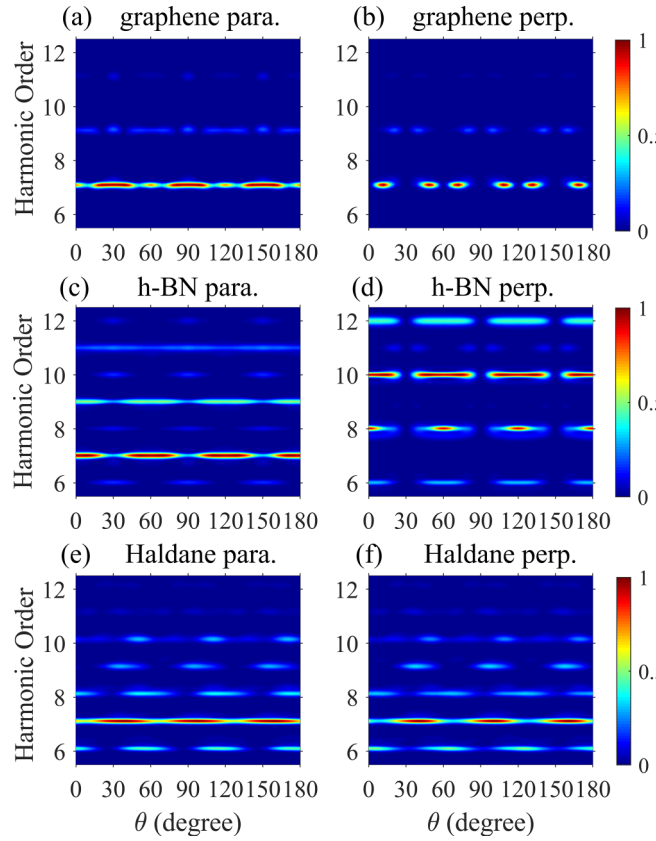

FIG. 2. Orientation dependence and polarization characteristics. Parallel and perpendicular components of the SSHG for (a), (b) graphene, (c), (d) h-BN, and (e), (f) Haldane model. The harmonic intensity is normalized.

In addition, the mirror symmetry can also induce destructive interference of harmonics as we derived by Eq. (10). When the driving laser is oriented parallel to the mirror plane ($\theta = 30° \pm 60°l$, $l \in \mathbb{N}$), there are no harmonics of perpendicular polarization because the currents cancel each other out. When the laser field is perpendicular to the mirror plane ($\theta = 60° \pm 60°l$, $l \in \mathbb{N}$), it strictly follows that only odd-order harmonics are generated for the parallel polarization and even-order harmonics for the perpendicular polarization. This tendency may spread to other general orientation angles, where the mirror symmetry is slightly broken. Time-reversal symmetry of crystal can also cause this tendency, but not strictly [7]. In addition, notice that although the h-BN only has an in-plane C_3 symmetry, the harmonics can form sixfold orientation periodicity. This can be completely attributed to the multicycle driving field usually used. The reversal of a multicycle laser field, equivalent to its carrier envelope phase

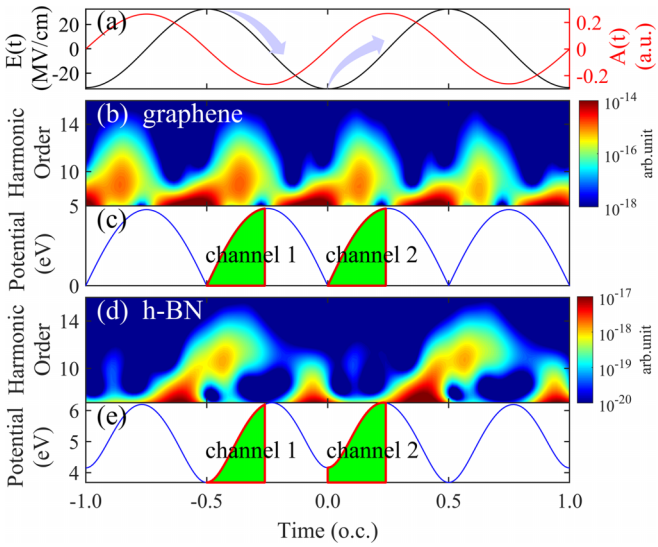

FIG. 3. Effect of photocurrent phase on harmonic radiation in time domain. (a) Electric field and vector potential of laser, the arrow indicates two adjacent electron channels, separated by half optical cycle. (b), (d) Time-frequency analysis for graphene and h-BN. (c), (e) Time-dependent laser-dressed effective potential between electron and hole excited at K point for graphene and h-BN. Integrals of the potential curves in the time domain are the photocurrent phases, which are marked by green regions for two interference channels. Laser polarization is along the Γ-M direction, the polarization of harmonics is parallel to the laser.

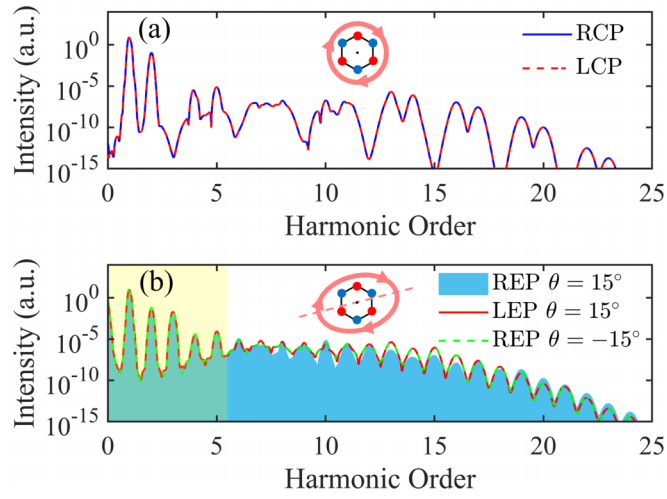

FIG. 4. (a) SSHG of h-BN driven by right-handed circularly polarized (RCP) and left-handed circularly polarized (LCP) light. (b) SSHG of h-BN driven by elliptically polarized light (the ellipticity of REP is 0.5, and LEP is -0.5), θ is the orientation angle between the main axis of ellipse and Γ-K direction. The harmonic intensity driven by left-handed elliptically polarized (LEP) light with $\theta = 15°$ (red solid line) is the same as that driven by right-handed elliptically polarized (REP) light with $\theta = -15°$ (green dashed line), but the REP case with $\theta = 15°$ (blue area) is offset from them in the high-order region.

shifts π, does not affect the overall intensity of harmonics. If a few-cycle driving field is used, such extra twofold orientation periodicity of harmonics cannot be observed. Therefore, a few-cycle driving probe is needed to determine the rotation axis of crystals.

To further discuss the effect of the mirror symmetry and time-reversal symmetry breaking, we consider the Haldane model with magnetic phase on the next-nearest-neighbor sites. The Hamiltonian is expanded as

$$H = t_1 \sum_{\langle i,j\rangle} c_i^\dagger c_j + M \sum_i \epsilon_i c_i^\dagger c_i + t_2 \sum_{\langle\langle i,j\rangle\rangle} e^{-iv_{ij}\varphi} c_i^\dagger c_j, \quad (20)$$

where $v_{ij} = \pm 1$ depending on the kind of atoms that the hopping takes place between. Here, we do not care about the optical behavior of its topological properties; the complex hopping strength is considered only to break the mirror and time-reversal symmetries. The basic point-group symmetry of this Hamiltonian is reduced to C_{3h}. The complex hopping strength $t_2 = 0.63$ eV, its phase $\varphi = \frac{\pi}{2}$. Since the mirrors are broken, the stable destructive and constructive interference that occur in the h-BN case vanishes in the Haldane model [see $\theta = \pm 30° l$, $l \in \mathbb{N}$ in Figs. 2(e) and 2(f)]. The spectra keep the orientation periodicity of 60°, which arises from the C_3 axis and the multicycle driving field.

B. Ellipticity dependence

The helicity dependence of SSHG can be used to probe molecular chirality, which is attributed to the circular dichroism of chiral molecules [43]. The similar thing happens in crystals: the mirror symmetry can protect the harmonics from the circular dichroism. Let us apply a helically polarized laser to a crystal with mirror symmetry. Under the mirror reflection, the applied right-hand helically polarized (σ_+) laser is changed to left-hand helically polarized (σ_-) laser. The photocurrent has

$$\hat{M}_c \mathbf{J}^a_{\sigma_+}(t) \hat{M}_c^\dagger = \mathbf{J}^{M_c^{-1}a}_{\sigma_-}(t) = M_{ca} \mathbf{J}^a_{\sigma_+}(t), \quad (21)$$

where c is the normal direction of mirror plane, and $M_{ca} = e^{i(\phi^{M_c^{-1}a}_{nm} - \phi^a_{nm})}$. In other words, the mirror reflection of the laser-crystal system directly causes the reflection of photocurrent. Therefore, there is no circular dichroism in SSHG from crystals with mirror symmetry. As Fig. 4(a) shows, the harmonic spectrum of h-BN driven by circularly polarized lights with inverse helicities has the same intensity. Due to the C_3 symmetry of the h-BN and the circularly polarized driving laser we used here, only $3l \pm 1 (l \in \mathbb{N})$ harmonic orders are allowed.

However, an asymmetric profile of elliptically dependent SSHG from cubic crystals has been demonstrated in Refs. [48–50], which was explained by the coupled intraband and interband dynamics. We find that this phenomenon is neither interband and intraband interference nor intraband contribution. Figure 5 shows the interband and intraband harmonics of h-BN under elliptically polarized laser with ellipticity ± 0.5. Whether in the low-order or high-order region, the interband and intraband components have the same feature for their elliptical dichroism. Here, we attribute this asymmetry to the mirror reflection mismatch between light field and crystal. The elliptical dichroism may be induced if only the helicity of elliptically polarized light is reversed while its orientation angle remains [see the difference in high-order

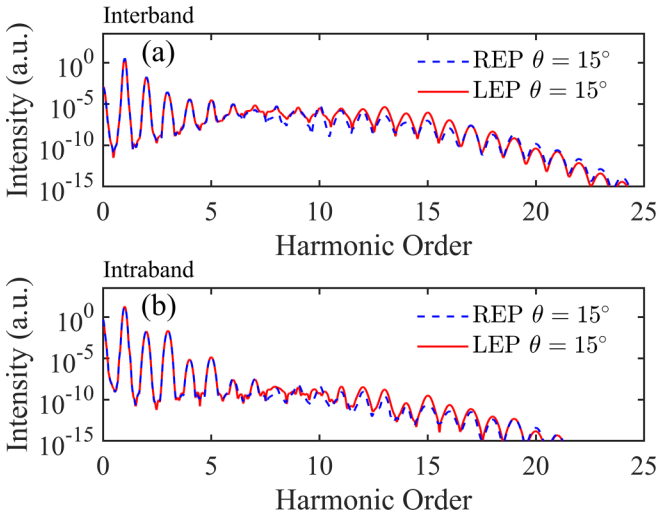

FIG. 5. Interband (a) and intraband (b) SSHG of h-BN driven by right-handed elliptically polarized (REP) and left-handed elliptically polarized (LEP) light (the ellipticity of REP is 0.5, and LEP is −0.5), θ is the orientation angle between the main axis of ellipse and Γ-K direction.

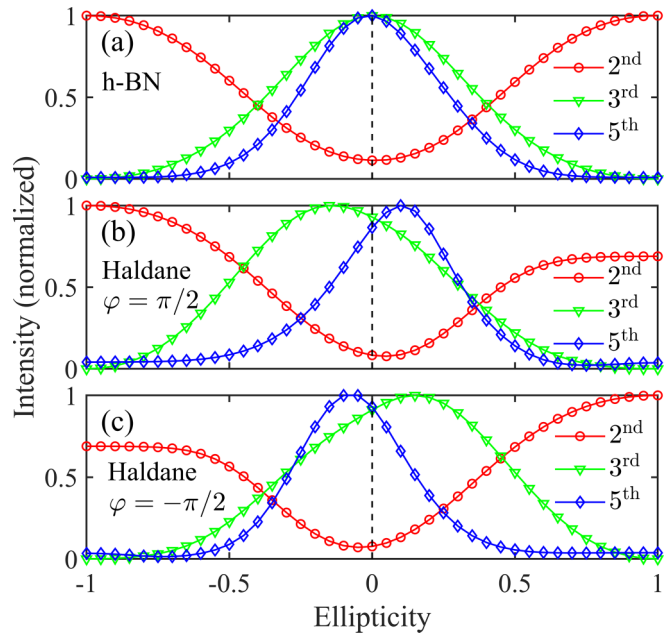

FIG. 6. Ellipticity dependence of low-order harmonic intensity for h-BN (a) and Haldane model with $\varphi = \pi/2$ (b), $\varphi = -\pi/2$ (c). The orientation angle θ is set to be 15°, other parameters of the models and laser are the same as Fig. 2. The intensity values are normalized for the second, third, and fifth harmonics.

region between the blue area and red solid line in Fig. 4(b)]. When we reflect the laser-crystal system simultaneously, the elliptical dichroism will vanish [see the red solid line and green dashed line in Fig. 4(b)].

The time-reversal symmetry can also reverse the helicity of in-plane laser fields. We can use the elliptical dichroism of harmonics to identify the time-reversal symmetry of crystals. We note the area shaded yellow in Fig. 4(b) that the low-order harmonics, nearly below band gap, never exhibit elliptical dichroism in h-BN. However, a completely different phenomenon emerges in the Haldane model with breaking time-reversal symmetry.

We deduce from Eq. (17) that the time-reversal symmetry of crystals prevents the low-order harmonics from the circular dichroism. In order to exclude the effect of mirror symmetry, we use an elliptically polarized laser and set the orientation angle to 15°. Expectedly, the low-order harmonics of h-BN keeps perfect ellipticity-dependent symmetry [see Fig. 6(a)]. However, due to the absence of the time-reversal symmetry, asymmetric ellipticity dependence can be clearly seen in the Haldane model [see Fig. 6(b)]. Thus, the elliptical dichroism of harmonics can be used to identify magnetic materials.

Then we consider the time-reversal enantiomer by flipping the magnetic flux of the Haldane model. As Figs. 6(b) and 6(c) show, when the phase of the flux is inverted, the ellipticity dependence is reversed exactly as well. This is equivalent to performing $\hat{T}$ on the laser-crystal system, but the intensity of low-order harmonics is unaltered. Combined with ultrafast time-resolved spectra, it is promising that the low-order harmonics can be used to observe the magnetization degree of materials or ultrafast spin dynamics [51,52]. Compared to the magneto-optical Kerr effect, we have extended the magnetic detection method to the nonlinear optical regime.

To further observe the applicable range of elliptic dichroism, here we use $\mathrm{ED}_n = (I_n^{\mathrm{REP}} - I_n^{\mathrm{LEP}})/(I_n^{\mathrm{REP}} + I_n^{\mathrm{LEP}})$ to describe the elliptical dichroism (ED) of harmonics, where I_n is nth-order harmonic intensity. In Fig. 7, we plot the ED of h-BN and Haldane models. The vertical dotted line marks the position of Keldysh parameter $\gamma = 1$ (tunneling regime $\gamma \ll 1$, multiphoton regime $\gamma \gg 1$). At the multiphoton regime, the ED of the low-order harmonics of h-BN approaches to 0, and is very small even at high laser field larger than 2.5 V/Å ($\approx 8 \times 10^{13}$ W/cm^2) that enters into tunneling regime. By contrast, the Haldane model exhibits strong ED even at low

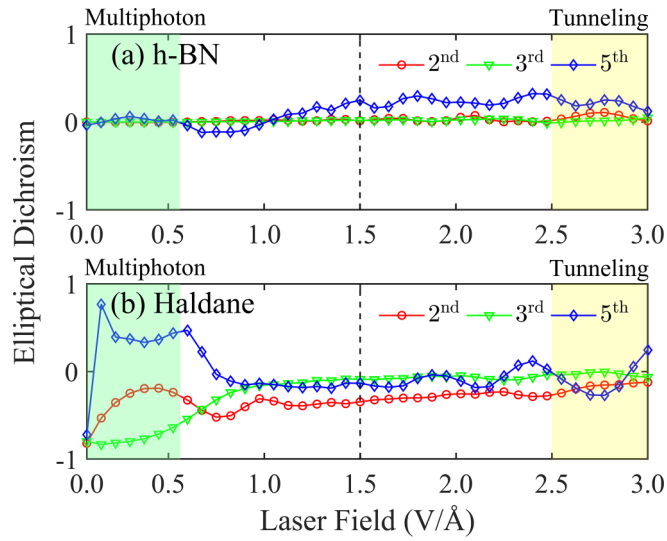

FIG. 7. Harmonic dichroism of h-BN (a) and Haldane model with $\varphi = \pi/2$ (b). The ellipticity of the driving laser used here is ±0.5. The vertical dotted line marks the position of Keldysh parameter $\gamma = 1$.

laser field less than 0.6 V/Å ($\approx 4 \times 10^{12}$ W/cm^2) in the multiphoton regime due to the time-reversal symmetry breaking. Therefore, the second-, third-, and fifth-order harmonics in multiphoton regime can be regarded as efficient optical signals to detect time-reversal symmetry breaking. Here it should be noted that the intensities of higher-order harmonics are normally very weak in multiphoton regime, and it is hard to utilize the ED of higher-order harmonics in this regard.

IV. CONCLUSIONS

In summary, we reorganize the formalism of laser-induced current, reveal the indispensable roles of the ΔTDP and shift phase, and provide a three-step picture based on laser-dressed bands for illustrating the interference process of SSHG. First, we point out that the selection rule of SSHG is determined by the ΔTDP under point-group symmetry operation. Second, in addition to the ΔTDP and the dynamical phase caused by the Coulomb field, the shift phase induced by the instantaneous potential of the oscillating laser is vital in SSHG. For example, when we reconstruct the band structure of noncentrosymmetric crystals and consider the propagation effect of SSHG or its phase-matching condition, the effects of the ΔTDP and shift phase are non-negligible [4,28]. Since the shift phase and the berry phase have a great relationship, we expect that this framework can promote SSHG for the characterization of topological band geometry [14,53]. The improved theoretical framework can help us to understand the microscopic mechanism of the selection rules, orientation dependence, polarization characteristics, time-frequency features, and ellipticity dependence of SSHG. Moreover, we derive that the low-order harmonics do not show elliptical dichroism in nonmagnetic systems, thus, strong-field nonlinear optics hold the promise to identify the magnetization degree of materials. In addition, our discussion is limited to the photocurrent under the electric dipole approximation, which can be generalized to the electric quadrupole and magnetic dipole regimes. Last but not least, the single-electron framework is no longer suitable for systems with strongly correlated interaction, thus establishing an efficient model involving quasiparticle transitions becomes particularly urgent.

ACKNOWLEDGMENTS

We gratefully acknowledge the support of the National Key Research and Development Program of China (Grants No. 2022YFA1604301 and No. 2018YFA0305700), the NSF of China (Grants No. 11974185, No. 11704187, No. 11834004, No. 11925408, No. 11921004, No. 12188101, No. 12174195, and No. 12304378), the Natural Science Foundation of Jiangsu Province (Grant No. BK20170032), Fundamental Research Funds for the Central Universities (Grant No. 30920021153), the Project funded by China Postdoctoral Science Foundation (Grant No. 2019M661841), the Postgraduate Research Practice Innovation Program of Jiangsu Province (KYCX22_0419), the Strategic Priority Research Program of CAS (XDB33000000), and the K. C. Wong Education Foundation (Grant No. GJTD-2018-01). The authors thank G. Yuan, H. Pi, Y. Qiao, X. Zhang, Z. Wang, and L. Chi for useful discussions.

APPENDIX A: DERIVATION OF PHOTOCURRENT

Based on the single-electron and dipole approximations, we can directly write the time-dependent Hamiltonian of matter interacting with an external laser field (atomic units are used throughout unless otherwise stated)

$$\hat{H}(t) = \hat{H}_0(t) + \hat{H}_l(t), \quad \hat{H}_0 = -\tfrac{1}{2}\nabla_{\mathbf{r}}^2 + \hat{V}(\mathbf{r}),$$
$$\hat{H}_l(t) = \hat{\mathbf{r}} \cdot \mathbf{E}(t), \tag{A1}$$

where $\nabla_{\mathbf{r}}^2$ is the Laplace operator with respect to the electronic coordinate operator $\hat{\mathbf{r}}$, $V(\mathbf{r})$ is the Coulomb potential, and $\mathbf{E}(t)$ is the applied electric field. It can be seen that the laser field only acts on the coordinate operators of a single electron without changing the Hamiltonian $\hat{H}_0$ of the initial system. In crystals, $V(\mathbf{r})$ has the translational symmetry, and electrons in the periodic lattice potential can be described by a wave packet composed of Bloch waves,

$$\psi(\mathbf{r}, t) = \frac{1}{N_c^{1/2}} \sum_m \int_{\mathrm{BZ}} d\mathbf{k}\, a_{m,\mathbf{k}}(t)\phi_{m,\mathbf{k}}(\mathbf{r}) \tag{A2}$$

with $\phi_{m,\mathbf{k}}(\mathbf{r}) = e^{i\mathbf{k}\mathbf{r}}u_{m,\mathbf{k}}(\mathbf{r})$, here $u_{m,\mathbf{k}}(\mathbf{r})$ is the periodic part of the Bloch wave function. N_c is the total number of unit cells, $a_{m,\mathbf{k}}(t)$ is the time-dependent probability amplitude of the Bloch wave. By using the time-dependent Schrödinger equation $i\frac{\partial\psi(\mathbf{r},t)}{\partial t} = H(t)\psi(\mathbf{r}, t)$, we can obtain

$$i\frac{\partial a_{n,\mathbf{k}'}(t)}{\partial t} = \varepsilon_{n,\mathbf{k}'}a_{n,\mathbf{k}'}(t) + \mathbf{E}(t) \cdot \sum_m \int_{\mathrm{BZ}} d\mathbf{k}\, a_{m,\mathbf{k}}(t)\langle\phi_{n,\mathbf{k}'}|\hat{\mathbf{r}}|\phi_{m,\mathbf{k}}\rangle, \tag{A3}$$

where the position operator under Bloch basis can be rewritten as $\langle\phi_{n,\mathbf{k}'}|\hat{\mathbf{r}}|\phi_{m,\mathbf{k}}\rangle = \delta(\mathbf{k}' - \mathbf{k})[-i\delta_{n,m}\partial_{\mathbf{k}'} + \mathbf{d}_{nm}(\mathbf{k}))]$, here the transition dipole matrix element $\mathbf{d}_{nm}(\mathbf{k}) = i\langle u_{n,\mathbf{k}}|\partial_{\mathbf{k}}|u_{m,\mathbf{k}}\rangle$ is introduced to describe the polarization of electron-hole pairs. Equation (A3) can be converted to the Houston basis after gauge transformations

$$i\frac{\partial a_{n,\mathbf{k}(t)}(t)}{\partial t} = \mathbf{E}(t) \cdot \sum_m \mathbf{d}_{nm}[\mathbf{k}(t)]a_{m,\mathbf{k}(t)}(t)e^{i\int_{-\infty}^{t}\varepsilon_{nm}[\mathbf{k}(\tau)]d\tau}, \tag{A4}$$

where $\varepsilon_{nm}(\mathbf{k}) = \varepsilon_n(\mathbf{k}) - \varepsilon_m(\mathbf{k})$ is the energy difference between bands. The quasimomentum $\mathbf{k}(t)$ of electrons changes adiabatically with the laser field, and the evolution relationship is $\mathbf{k}(t) = \mathbf{K} + \mathbf{A}(t)$. $\mathbf{K}$ is the canonical momentum of the crystal in the absence of field. This is a multiband coupling equation, in which the probability amplitude of the electron in the nth eigenstate is related to other states through the transition dipole moments. Equation (A4) can be regarded as a linear superposition of these transition processes, which form a statistical ensemble.

We introduce density matrix $\rho_{nm}(\mathbf{K}, t) = a^{\dagger}_{n,\mathbf{k}(t)}(t)a_{m,\mathbf{k}(t)}(t)$ to describe the time-dependent evolution of the electronic population. For simplicity, here we consider the population

transition that occurs mainly between two bands, which can always be described by a two-band equation. The densities of interband and intraband currents obey (we ignore the dephasing time related to coupling between particles)

$$\dot{\rho}_{nm}(\mathbf{K},t) = -i\mathbf{E}(t)\cdot[\{\mathbf{d}_{mm}[\mathbf{k}(t)]-\mathbf{d}_{nn}[\mathbf{k}(t)]\}\rho_{nm}(\mathbf{K},t)+\mathbf{d}_{mn}[\mathbf{k}(t)]f_{nm}(\mathbf{K},t)e^{i\int_{-\infty}^{t}\varepsilon_{mn}[\mathbf{k}(\tau)]d\tau}], \tag{A5}$$

$$\dot{\rho}_{nn}(\mathbf{K},t) = -i\mathbf{E}(t)\cdot\mathbf{d}_{nm}[\mathbf{k}(t)]\rho_{nm}(\mathbf{K},t)e^{i\int_{-\infty}^{t}\varepsilon_{nm}[\mathbf{k}(\tau)]d\tau}+\text{c.c.}, \tag{A6}$$

where $f_{nm}(\mathbf{K},t)=\rho_{nn}(\mathbf{K},t)-\rho_{mm}(\mathbf{K},t)$ is the difference of Fermi-Dirac distribution, and the band index $n\neq m$. Equations (A5) and (A6) are results of the coupling between the adiabatic evolution and nonadiabatic tunneling process of the electron density. The time-dependent photocurrent can be divided into interband and intraband components:

$$\mathbf{J}_{nm}(t) = -\frac{1}{N_c}\sum_{\mathbf{K}\in\mathrm{BZ}}\rho_{nm}(\mathbf{K},t)\mathbf{p}_{nm}[\mathbf{k}(t)], \tag{A7}$$

$$\mathbf{J}_{nn}(t) = -\frac{1}{N_c}\sum_{\mathbf{K}\in\mathrm{BZ}}\rho_{nn}(\mathbf{K},t)\mathbf{p}_{nn}[\mathbf{k}(t)], \tag{A8}$$

where the momentum operator can be given by $\hat{\mathbf{p}}(\mathbf{k},t)=\partial_{\mathbf{k}}\hat{H}(\mathbf{k},t)$. In this paper, we assume the evolution of the electron population has no effect on the Coulomb potential. Therefore, the original Hilbert space does not change with the addition of laser fields. The momentum matrix element takes the form $\mathbf{p}_{nm}(\mathbf{k})=\langle u_{n,\mathbf{k}}|\hat{\mathbf{p}}|u_{m,\mathbf{k}}\rangle$, which can be calculated by

$$\mathbf{p}_{nm}(\mathbf{k}) = i\varepsilon_{nm}(\mathbf{k})\mathbf{d}_{nm}(\mathbf{k}), \quad n\neq m \tag{A9}$$

$$\mathbf{p}_{nn}(\mathbf{k}) = \partial_{\mathbf{k}}\varepsilon_n(\mathbf{k}). \tag{A10}$$

The anomalous velocity induced by the Berry curvature has been included in Eq. (A7). Then, we can obtain expressions for the interband and intraband currents as Eqs. (1) and (2).

APPENDIX B: TRANSFORMATION OF TRANSITION DIPOLE UNDER POINT-GROUP SYMMETRY

Consider a point-group symmetry operation $\hat{G}$ on the Bloch state of electrons,

$$\hat{G}|u_{n,\mathbf{k}}\rangle = |u_{n,G^{-1}\mathbf{k}}\rangle. \tag{B1}$$

For the transition dipole matrix element, we have

$$\begin{aligned}\hat{G}\mathbf{d}^{a}_{nm}(\mathbf{k})\hat{G}^{\dagger} &= i\hat{G}\langle u_{n,\mathbf{k}}|\partial_{\mathbf{k}_a}|u_{m,\mathbf{k}}\rangle\hat{G}^{\dagger}\\ &= i\langle u_{n,G^{-1}\mathbf{k}}|\hat{G}\partial_{\mathbf{k}_a}\hat{G}^{\dagger}|u_{m,G^{-1}\mathbf{k}}\rangle\\ &= i\langle u_{n,G^{-1}\mathbf{k}}|\partial_{(G^{-1}\mathbf{k})_{a'}}|u_{m,G^{-1}\mathbf{k}}\rangle\\ &= \mathbf{d}^{a'}_{nm}(G^{-1}\mathbf{k}),\end{aligned} \tag{B2}$$

where $a,a'=G^{-1}a$ denote the directions of the transition dipole moments. If the crystal has G symmetry, its Hamiltonian satisfies $\hat{G}\hat{H}=\hat{H}\hat{G}$, the Bloch wave is thus the eigenstate of $\hat{G}$ as well. Since $\hat{G}$ is unitary, its eigenvalues are complex numbers of modulo 1:

$$\hat{G}|u_{n,\mathbf{k}}\rangle = e^{i\phi_G}|u_{n,\mathbf{k}}\rangle. \tag{B3}$$

Thus, we obtain $|u_{n,G^{-1}\mathbf{k}}\rangle = e^{i\phi_G}|u_{n,\mathbf{k}}\rangle$. Then,

$$\begin{aligned}\mathbf{d}^{a'}_{nm}(G^{-1}\mathbf{k}) &= i\langle u_{n,\mathbf{k}}|\partial_{(G^{-1}\mathbf{k})_{a'}}|u_{m,\mathbf{k}}\rangle\\ &= ie^{i[\phi^{a'}_{nm}[\mathbf{k}(t)]-\phi^{a}_{nm}(\mathbf{k}(t))]}\langle u_{n,\mathbf{k}}|\partial_{\mathbf{k}_a}|u_{m,\mathbf{k}}\rangle\\ &= G_{a'a}\mathbf{d}^{a}_{nm}(\mathbf{k}),\end{aligned} \tag{B4}$$

in which $G_{a'a}$ is just the ΔTDP between a and a' directions under $\hat{G}$. Moreover, scalar quantities such as the dynamical phase and shift phase are invariant under $\hat{G}$.

APPENDIX C: TYPICAL CASES OF SELECTION RULES OF SHG

1. Mirror symmetry

A twofold mirror dynamical symmetry can be obtained by exciting the dipole pairs with oscillating electric field which is symmetric about a mirror plane. Adjoining order-2 temporal operator $\hat{\tau}_2$ with the mirror reflection $\hat{M}_c$, we define the dynamical symmetry operation $\hat{F}=\hat{M}_c\cdot\hat{\tau}_2$, where c is the normal direction of the mirror plane. Monochromatic lights reverse along c under $\hat{\tau}_2$ [i.e., $\hat{\tau}_2\mathbf{E}^c(t)=-\mathbf{E}^c(t)$], so we have $\hat{F}\mathbf{k}(t)=M_c^{-1}\mathbf{K}+\mathbf{A}(\hat{\tau}_2 t)=M_c^{-1}\mathbf{k}(t)$. According to Eq. (10), we derive that the interband photocurrent transforms as

$$\begin{aligned}&\hat{F}\mathbf{J}^{a}_{nm}(\mathbf{K},t)\hat{F}^{\dagger}\\ &= \mathbf{J}^{M_c^{-1}a}_{nm}\left(M_c^{-1}\mathbf{K},\hat{\tau}_2 t\right)\\ &= -i\varepsilon_{nm}\left(M_c^{-1}\mathbf{k}(t)\right)\mathbf{d}^{M_c^{-1}a}_{nm}\left(M_c^{-1}\mathbf{k}(t)\right)\rho_{nm}\left(M_c^{-1}\mathbf{K},\hat{\tau}_2 t\right)\\ &= -i\varepsilon_{nm}[\mathbf{k}(t)]\mathbf{d}^{a}_{nm}[\mathbf{k}(t)]e^{i\left[\phi^{M_c^{-1}a}_{nm}[\mathbf{k}(t)]-\phi^{a}_{nm}[\mathbf{k}(t)]\right]}\rho_{nm}(\mathbf{K},t).\end{aligned} \tag{C1}$$

When $a\parallel c$, the ΔTDP is $\phi^{M_c^{-1}a}_{nm}(\mathbf{k})-\phi^{a}_{nm}(\mathbf{k})=\pi$. Thus, the photocurrent satisfies $\hat{F}\mathbf{J}^{a}_{nm}(t)\hat{F}^{\dagger}=-\mathbf{J}^{a}_{nm}(t)$. Such reversal of the current only comes from the reflected dipole moment $\mathbf{d}^{a}_{nm}$. This Floquet system can be reduced to two pairs of electric dipoles with opposing polarization directions and separated by half an optical cycle (o.c.) in the time domain [see Fig. 1(a)].

The photons with frequency ω become interference enhanced if the current satisfies $\hat{F}\mathbf{J}^{a}_{nm}(\omega)\hat{F}^{\dagger}=\mathbf{J}^{a}_{nm}(\omega)$. Using the Fourier transform that $\mathbf{J}^{a}_{nm}(\omega)=\int_{-\infty}^{+\infty}dt\,\mathbf{J}^{a}_{nm}(t)e^{i\omega t}$, we have

$$e^{i\omega\frac{T_0}{2}} = e^{i\pi} \Rightarrow \omega=(2l+1)\omega_0, \quad l\in\mathbb{N} \tag{C2}$$

where $\mathbb{N}$ denotes natural numbers. Considering similar transformation for Eq. (2) corresponding to intraband current, we can easily reach the same conclusion. Therefore, when the

laser field is perpendicular to the mirror plane, only odd-order harmonics emit in the direction parallel to the driving field.

When $a \perp c$, the ΔTDP is $\phi^{M_c^{-1}a}_{nm}(\mathbf{k}) - \phi^{a}_{nm}(\mathbf{k}) = 0$. The photocurrent satisfies $\mathbf{J}^{M_c^{-1}a}(\hat{\tau}_2 t) = \mathbf{J}^a(t)$. This derives only even-order harmonic generation in the direction perpendicular to the driving field ($\omega = 2l\omega_0,\ l \in \mathbb{N}$). Applying linearly polarized laser parallel to the mirror plane does not break the mirror symmetry of the system, i.e., $\hat{M}_c \hat{H}(t) \hat{M}_c^\dagger = \hat{H}(t)$. The current perpendicular to the mirror plane meets $\hat{M}_c \mathbf{J}^a(\mathbf{K}, t) \hat{M}_c^\dagger = \mathbf{J}^{M_c^{-1}a}(M_c^{-1}\mathbf{K}, t) = -\mathbf{J}^a(\mathbf{K}, t)$. Here, the reverse current also comes from the reflection of the transition dipole moment. Since the currents on both sides of the mirror are opposite, it is concluded that when the driving light is parallel to the mirror plane, no harmonics can be generated perpendicular to the mirror plane (relevant rules are presented in Table I of main text).

2. Rotational symmetry

Pure rotational symmetry usually exists in a two-dimensional plane; there are only five types of rotation axes in crystals (onefold, twofold, threefold, fourfold, and sixfold) due to periodic translational symmetry of lattices. Combining order-N temporal operator $\hat{\tau}_N$ and N-fold rotational symmetry operator $\hat{C}_N$, we define a dynamical symmetry operation $\hat{R}_N = \hat{C}_N \cdot \hat{\tau}_N$. When a laser field with R_N symmetry acts on a crystal with C_N symmetry (considering the plane of electric field is always perpendicular to the C_N axis), we have $\hat{R}_N \mathbf{k}(t) = C_N^{-1}\mathbf{K} + \mathbf{A}(\hat{\tau}_N t) = C_N^{-1}\mathbf{k}(t)$, this system can form a dynamical symmetry. The interband current transforms as

$$\begin{aligned}\hat{R}_N \mathbf{J}^a_{nm}(\mathbf{K}, t) \hat{R}_N^\dagger &= \mathbf{J}^{C_N^{-1}a}_{nm}\left(C_N^{-1}\mathbf{K}, \hat{\tau}_N t\right) \\ &= -i\varepsilon_{nm}\left(C_N^{-1}\mathbf{k}(t)\right)\mathbf{d}^{C_N^{-1}a}_{nm}\left(C_N^{-1}\mathbf{k}(t)\right)\rho_{nm}\left(C_N^{-1}\mathbf{K}, \hat{\tau}_N t\right) \\ &= -i\varepsilon_{nm}[\mathbf{k}(t)]\mathbf{d}^a_{nm}[\mathbf{k}(t)] e^{i\left[\phi^{C_N^{-1}a}_{nm}[\mathbf{k}(t)] - \phi^a_{nm}[\mathbf{k}(t)]\right]}\rho_{nm}(\mathbf{K}, t).\end{aligned} \tag{C3}$$

Let us first consider the in-plane polarization. Since the rotational symmetry operator has two eigenvalues $e^{\pm i\frac{2\pi}{N}}$, the ΔTDP should be $\phi^{C_N^{-1}a}_{nm}(\mathbf{k}) - \phi^a_{nm}(\mathbf{k}) = \pm\frac{2\pi}{N}$, denoting the rotation angle of dipoles under $\hat{C}_N$ [see Fig. 1(b) for the case of $N = 3$]. Thus, integrating over the entire BZ, we can obtain $\hat{R}_N \mathbf{J}^a_{nm}(t) \hat{R}_N^\dagger = e^{\pm i\frac{2\pi}{N}} \mathbf{J}^a_{nm}(t)$. Using the interference form of the Fourier transform that $\hat{R}_N \mathbf{J}^a_{nm}(\omega) \hat{R}_N^\dagger = \mathbf{J}^a_{nm}(\omega)$, we know that the frequency of photons emitted perpendicular to the rotation axis can only be $\omega = (Nl \pm 1)\omega_0,\ l \in \mathbb{N}$, which corresponds to corotating and counter-rotating photons relative to driving lasers, respectively. A same result can be obtained for the intraband current.

For the out-plane polarization, we have $\hat{R}_N \mathbf{J}^a(\mathbf{K}, t) \hat{R}_N^\dagger = \mathbf{J}^a(\mathbf{K}, t)$. Thus, the frequency of photons emitted parallel to the rotation axis can only be $\omega = Nl\omega_0,\ l \in \mathbb{N}$. When the electric field is parallel to the rotation axis, the rotational symmetry of the system is always maintained, i.e., $\hat{C}_N \hat{H}(t) \hat{C}_N^\dagger = \hat{H}(t)$. The photocurrent perpendicular to the axis satisfies $\hat{C}_N \mathbf{J}^a(\mathbf{K}, t) \hat{C}_N^\dagger = \mathbf{J}^{C_N^{-1}a}(C_N^{-1}\mathbf{K}, t) = e^{\pm i\frac{2\pi}{N}} \mathbf{J}^{C_N^{-1}a}(C_N^{-1}\mathbf{K}, t)$. Then we get $e^{\pm i\frac{2\pi}{N}} = 1 \Rightarrow N = 1$. In other words, when the electric field is always parallel to the N-fold ($N \geqslant 2$) rotation axis, no current generates perpendicular to the axis (relevant rules are presented in Table II of the main text).

APPENDIX D: DERIVATION OF EQS. (12) AND (17)

We now derive the optical response induced by crystal time-reversal symmetry. For the proof of Eq. (12), considering time-reversal operation $\hat{T}$ on the Bloch state of electrons,

$$\hat{T}|u_{n,\mathbf{k}}\rangle = |u_{n,-\mathbf{k}}\rangle^*. \tag{D1}$$

Thus, for transition dipole matrix elements,

$$\begin{aligned}\hat{T}\mathbf{d}^a_{nm}(\mathbf{k})\hat{T}^\dagger &= \hat{T}\langle u_{n,\mathbf{k}}|i\partial_{\mathbf{k}_a}|u_{m,\mathbf{k}}\rangle\hat{T}^\dagger \\ &= -i\langle \partial_{-\mathbf{k}_a} u_{m,-\mathbf{k}} \mid u_{n,-\mathbf{k}}\rangle \\ &= i\langle u_{m,-\mathbf{k}}|\partial_{-\mathbf{k}_a}|u_{n,-\mathbf{k}}\rangle \\ &= \mathbf{d}^a_{mn}(-\mathbf{k}).\end{aligned} \tag{D2}$$

If the system has time-reversal symmetry (i.e., $\hat{T}\hat{H} = \hat{H}\hat{T}$), the Bloch wave is the eigenstate of $\hat{T}$ as well. Due to the antiunitarity of $\hat{T}$, its eigenvalues are complex numbers of modulo 1:

$$\hat{T}|u_{n,\mathbf{k}}\rangle = e^{i\phi_\mathbf{k}}|u_{n,\mathbf{k}}\rangle. \tag{D3}$$

Therefore, we have $|u_{n,-\mathbf{k}}\rangle^* = e^{i\phi_\mathbf{k}}|u_{n,\mathbf{k}}\rangle$. Then,

$$\begin{aligned}\mathbf{d}^a_{mn}(-\mathbf{k}) &= -i\langle \partial_{-\mathbf{k}_a} u_{m,-\mathbf{k}} \mid u_{n,-\mathbf{k}}\rangle \\ &= i\langle u_{n,\mathbf{k}}|\partial\mathbf{k}_a|u_{m,\mathbf{k}}\rangle \\ &= \mathbf{d}^a_{nm}(\mathbf{k}).\end{aligned} \tag{D4}$$

Similarly, we can obtain the constraints of time-reversal symmetry on the band dispersion and the shift vector, respectively:

$$\begin{aligned}\hat{T}\varepsilon_n(\mathbf{k})\hat{T}^\dagger &= \varepsilon_n(-\mathbf{k}) = \varepsilon_n(\mathbf{k}), \\ \hat{T}\mathbf{R}^{a,b}_{nm}(\mathbf{k})\hat{T}^\dagger &= \mathbf{R}^{a,b}_{nm}(-\mathbf{k}) = \mathbf{R}^{a,b}_{nm}(\mathbf{k}).\end{aligned} \tag{D5}$$

Similar to the case of inversion symmetry, we define an operator $\hat{U}$ that performs $\hat{T}$ on the crystals, and order-2 temporal operator $\hat{\tau}_2$ on the time. The time-dependent quasimomentum has $\hat{U}\mathbf{k}(t) = -\mathbf{k}(t)$. The dynamical phase, shift phase, and ΔTDP transform as

$$\begin{aligned}\hat{U}S_{\text{dyn}}(\mathbf{K}, t, t')\hat{U}^\dagger &= S_{\text{dyn}}(-\mathbf{K}, \hat{\tau}_2 t, \hat{\tau}_2 t') \\ &= S_{\text{dyn}}(\mathbf{K}, t, t'), \\ \hat{U}S_{\text{shift}}(\mathbf{K}, t, t')\hat{U}^\dagger &= S_{\text{shift}}(-\mathbf{K}, \hat{\tau}_2 t, \hat{\tau}_2 t') \\ &= -S_{\text{shift}}(\mathbf{K}, t, t'), \\ \hat{U}S_{\Delta\text{TDP}}(\mathbf{k}(t))\hat{U}^\dagger &= S_{\Delta\text{TDP}}[-\mathbf{k}(t)] \\ &= -S_{\Delta\text{TDP}}[\mathbf{k}(t)].\end{aligned} \tag{D6}$$

Combining the point-group symmetry,

$$\begin{aligned}\hat{P}S_{\text{shift}}(\mathbf{K}, t, t')\hat{P}^\dagger &= S_{\text{shift}}(-\mathbf{K}, \hat{\tau}_2 t, \hat{\tau}_2 t') \\ &= S_{\text{shift}}(\mathbf{K}, t, t'),\end{aligned} \tag{D7}$$

we know that the S_{shift} vanish in crystals that both time-reversal symmetry and inversion symmetry are satisfied. Therefore, it could be reasonable to consider only the dynamical phase at this time. Of course, when considering the harmonics that are not collinear with the laser field, ΔTDP exactly cannot be ignored.

The interband current under $\hat{U}$ takes

$$\begin{aligned}\hat{U}\mathbf{J}^a_{nm}(\mathbf{K},t)\hat{U}^\dagger &= \mathbf{J}^a_{nm}(-\mathbf{K},\hat{\tau}_2 t)\\ &= -\int_{-\infty}^{\hat{\tau}_2 t} d\hat{\tau}_2 t' \varepsilon_{nm}[-\mathbf{k}(t)]|\mathbf{d}^a_{nm}[-\mathbf{k}(t)]|\\ &\quad\times\left[\mathbf{E}^b(\hat{\tau}_2 t')\cdot\left|\mathbf{d}^b_{mn}[-\mathbf{k}(t')]\right|\right] f_{nm}(-\mathbf{K},\hat{\tau}_2 t)\\ &\quad\times e^{-i\left[S_{\rm dyn}(-\mathbf{K},\hat{\tau}_2 t,\hat{\tau}_2 t')+S_{\rm shift}(-\mathbf{K},\hat{\tau}_2 t,\hat{\tau}_2 t')+S_{\Delta\rm TDP}[-\mathbf{k}(t)]\right]}\\ &= \int_{-\infty}^{t} dt' \varepsilon_{nm}[\mathbf{k}(t)]|\mathbf{d}^a_{mn}[\mathbf{k}(t)]|\left[\mathbf{E}^b(t')\cdot\left|\mathbf{d}^b_{nm}[\mathbf{k}(t')]\right|\right]\\ &\quad\times f_{nm}(\mathbf{K},t)e^{-i\left[S_{\rm dyn}(\mathbf{K},t,t')-S_{\rm shift}(\mathbf{K},t,t')-S_{\Delta\rm TDP}[\mathbf{k}(t)]\right]}\\ &= -\mathbf{J}^a_{nm}(\mathbf{K},t)e^{2i[S_{\rm shift}(\mathbf{K},t,t')+S_{\Delta\rm TDP}[\mathbf{k}(t)]]}. \end{aligned} \tag{D8}$$

For the proof of Eq. (17),

$$\begin{aligned}\hat{T}\mathbf{J}^a_{nm,\sigma_+}(\mathbf{K},t)\hat{T}^\dagger &= \mathbf{J}^a_{nm,\sigma_-}(-\mathbf{K},-t) = -\int_{+\infty}^{-t} dt' \varepsilon_{nm}(-\mathbf{K}+\mathbf{A}_{\sigma_-}(-t))\left|\mathbf{d}^a_{nm}(-\mathbf{K}+\mathbf{A}_{\sigma_-}(-t))\right|\\ &\quad\times\left[\mathbf{E}^b_{\sigma_-}(t')\cdot\left|\mathbf{d}^b_{mn}(-\mathbf{K}+\mathbf{A}_{\sigma_-}(t'))\right|\right] f_{nm}(-\mathbf{K},-t)e^{-i\left[S_{\rm dyn}\left(-\mathbf{K},\mathbf{A}_{\sigma_-},-t,t'\right)+S_{\rm shift}\left(-\mathbf{K},\mathbf{A}_{\sigma_-}-t,t'\right)+S_{\Delta\rm TDP}\left(-\mathbf{K}+\mathbf{A}_{\sigma_-}(-t)\right)\right]}\\ &= \int_{-\infty}^{t} dt' \varepsilon_{nm}(\mathbf{K}+\mathbf{A}_{\sigma_+}(t))\left|\mathbf{d}^a_{mn}(\mathbf{K}+\mathbf{A}_{\sigma_+}(t))\right|\\ &\quad\times\left[\mathbf{E}^b_{\sigma_+}(t')\cdot\left|\mathbf{d}^b_{nm}(\mathbf{K}+\mathbf{A}_{\sigma_+}(t'))\right|\right] f_{nm}(-\mathbf{K},-t)e^{-i\left[-S_{\rm dyn}\left(\mathbf{K},\mathbf{A}_{\sigma_+},t,t'\right)-S_{\rm shift}\left(\mathbf{K},\mathbf{A}_{\sigma_+},t,t'\right)-S_{\Delta\rm TDP}\left(\mathbf{K}+\mathbf{A}_{\sigma_+}(t)\right)\right]}\\ &= -\mathbf{J}^{a,*}_{nm,\sigma_+}(\mathbf{K},t)\frac{f_{nm}(-\mathbf{K},-t)}{f_{nm}(\mathbf{K},t)}. \end{aligned} \tag{D9}$$

Here, the initial right-hand helically polarized laser (σ_+) is changed to left-hand helically polarized laser (σ_-) under the time-reversal transformation, which has $\mathbf{E}_{\sigma_+}(t)=\mathbf{E}_{\sigma_-}(-t)$ and $\mathbf{A}_{\sigma_+}(t)=-\mathbf{A}_{\sigma_-}(-t)$. In the second step, we have assumed that the pulse envelope is infinite; then the temporal integral from $-\infty$ is identical with that from $+\infty$. We use the transformation relations shown in Eqs. (14)–(16) in the third step. A derivation process for the intraband current is similar.

[1] A. H. Chin, O. G. Calderón, and J. Kono, Extreme midinfrared nonlinear optics in semiconductors, Phys. Rev. Lett. **86**, 3292 (2001).

[2] S. Ghimire, A. D. DiChiara, E. Sistrunk, P. Agostini, L. F. DiMauro, and D. A. Reis, Observation of high-order harmonic generation in a bulk crystal, Nat. Phys. **7**, 138 (2011).

[3] G. Vampa, T. J. Hammond, N. Thiré, B. E. Schmidt, F. Légaré, C. R. McDonald, T. Brabec, D. D. Klug, and P. B. Corkum, All-optical reconstruction of crystal band structure, Phys. Rev. Lett. **115**, 193603 (2015).

[4] L. Li, P. Lan, L. He, W. Cao, Q. Zhang, and P. Lu, Determination of electron band structure using temporal interferometry, Phys. Rev. Lett. **124**, 157403 (2020).

[5] A. J. Uzan-Narovlansky, Álvaro Jiménez-Galán, G. Orenstein, R. E. F. Silva, T. Arusi-Parpar, S. Shames, B. D. Bruner, B. Yan, O. Smirnova, M. Ivanov *et al.*, Observation of light-driven band structure via multiband high-harmonic spectroscopy, Nat. Photonics **16**, 428 (2022).

[6] D. Xiao, M.-C. Chang, and Q. Niu, Berry phase effects on electronic properties, Rev. Mod. Phys. **82**, 1959 (2010).

[7] H. Liu, Y. Li, Y. S. You, S. Ghimire, T. F. Heinz, and D. A. Reis, High-harmonic generation from an atomically thin semiconductor, Nat. Phys. **13**, 262 (2017).

[8] T. T. Luu and H. J. Wörner, Measurement of the Berry curvature of solids using high-harmonic spectroscopy, Nat. Commun. **9**, 916 (2018).

[9] Y.-Y. Lv, J. Xu, S. Han, C. Zhang, Y. Han, J. Zhou, S.-H. Yao, X.-P. Liu, M.-H. Lu, H. Weng *et al.*, High-harmonic generation in Weyl semimetal $\beta-\mathrm{WP}_2$ crystals, Nat. Commun. **12**, 6437 (2021).

[10] T. Morimoto and N. Nagaosa, Topological nature of nonlinear optical effects in solids, Sci. Adv. **2**, e1501524 (2016).

[11] R. Silva, Á. Jiménez-Galán, B. Amorim, O. Smirnova, and M. Ivanov, Topological strong-field physics on sub-laser-cycle timescale, Nat. Photonics **13**, 849 (2019).

[12] A. Chacón, D. Kim, W. Zhu, S. P. Kelly, A. Dauphin, E. Pisanty, A. S. Maxwell, A. Picón, M. F. Ciappina, D. E. Kim *et al.*, Circular dichroism in higher-order harmonic generation: Heralding topological phases and transitions in Chern insulators, Phys. Rev. B **102**, 134115 (2020).

[13] D. Baykusheva, A. Chacón, D. Kim, D. E. Kim, D. A. Reis, and S. Ghimire, Strong-field physics in three-dimensional topological insulators, Phys. Rev. A **103**, 023101 (2021).

[14] C. Qian, C. Yu, S. Jiang, T. Zhang, J. Gao, S. Shi, H. Pi, H. Weng, and R. Lu, Role of shift vector in high-harmonic generation from noncentrosymmetric topological insulators under strong laser fields, Phys. Rev. X **12**, 021030 (2022).

[15] H. K. Avetissian and G. F. Mkrtchian, Impact of electron-electron Coulomb interaction on the high harmonic generation process in graphene, Phys. Rev. B **97**, 115454 (2018).

[16] Y. Murakami, M. Eckstein, and P. Werner, High-harmonic generation in Mott insulators, Phys. Rev. Lett. **121**, 057405 (2018).

[17] R. Silva, I. V. Blinov, A. N. Rubtsov, O. Smirnova, and M. Ivanov, High-harmonic spectroscopy of ultrafast many-body dynamics in strongly correlated systems, Nat. Photonics **12**, 266 (2018).

[18] C. Shao, H. Lu, X. Zhang, C. Yu, T. Tohyama, and R. Lu, High-harmonic generation approaching the quantum critical point of strongly correlated systems, Phys. Rev. Lett. **128**, 047401 (2022).

[19] C. L. Tang and H. Rabin, Selection rules for circularly polarized waves in nonlinear optics, Phys. Rev. B **3**, 4025 (1971).

[20] N. Ben-Tal, N. Moiseyev, and A. Beswick, The effect of Hamiltonian symmetry on generation of odd and even harmonics, J. Phys. B: At., Mol. Opt. Phys. **26**, 3017 (1993).

[21] O. E. Alon, V. Averbukh, and N. Moiseyev, Selection rules for the high harmonic generation spectra, Phys. Rev. Lett. **80**, 3743 (1998).

[22] O. Neufeld, D. Podolsky, and O. Cohen, Floquet group theory and its application to selection rules in harmonic generation, Nat. Commun. **10**, 405 (2019).

[23] X. Liu, X. Zhu, L. Li, Y. Li, Q. Zhang, P. Lan, and P. Lu, Selection rules of high-order-harmonic generation: Symmetries of molecules and laser fields, Phys. Rev. A **94**, 033410 (2016).

[24] S. Qiao, L. Li, X. Zhu, P. Lan, and P. Lu, Resolving the polarization of high-order harmonic generation by temporal multislit interferometry, Phys. Rev. A **104**, 023114 (2021).

[25] K. Kaneshima, Y. Shinohara, K. Takeuchi, N. Ishii, K. Imasaka, T. Kaji, S. Ashihara, K. L. Ishikawa, and J. Itatani, Polarization-resolved study of high harmonics from bulk semiconductors, Phys. Rev. Lett. **120**, 243903 (2018).

[26] S. Jiang, J. Chen, H. Wei, C. Yu, R. Lu, and C. D. Lin, Role of the transition dipole amplitude and phase on the generation of odd and even high-order harmonics in crystals, Phys. Rev. Lett. **120**, 253201 (2018).

[27] C. Liu, Y. Zheng, Z. Zeng, and R. Li, Polarization-resolved analysis of high-order harmonic generation in monolayer MoS_2, New J. Phys. **22**, 073046 (2020).

[28] G. Vampa, C. R. McDonald, G. Orlando, D. D. Klug, P. B. Corkum, and T. Brabec, Theoretical analysis of high-harmonic generation in solids, Phys. Rev. Lett. **113**, 073901 (2014).

[29] S. Jiang, H. Wei, J. Chen, C. Yu, R. Lu, and C. D. Lin, Effect of transition dipole phase on high-order-harmonic generation in solid materials, Phys. Rev. A **96**, 053850 (2017).

[30] J. Li, X. Zhang, S. Fu, Y. Feng, B. Hu, and H. Du, Phase invariance of the semiconductor Bloch equations, Phys. Rev. A **100**, 043404 (2019).

[31] L. Yue and M. B. Gaarde, Imperfect recollisions in high-harmonic generation in solids, Phys. Rev. Lett. **124**, 153204 (2020).

[32] J. Wilhelm, P. Grössing, A. Seith, J. Crewse, M. Nitsch, L. Weigl, C. Schmid, and F. Evers, Semiconductor Bloch-equations formalism: Derivation and application to high-harmonic generation from Dirac fermions, Phys. Rev. B **103**, 125419 (2021).

[33] C. Yu, S. Jiang, and R. Lu, High order harmonic generation in solids: A review on recent numerical methods, Adv. Phys. X **4**, 1562982 (2019).

[34] R. E. F. Silva, F. Martín, and M. Ivanov, High harmonic generation in crystals using maximally localized Wannier functions, Phys. Rev. B **100**, 195201 (2019).

[35] L. Yue and M. B. Gaarde, Structure gauges and laser gauges for the semiconductor Bloch equations in high-order harmonic generation in solids, Phys. Rev. A **101**, 053411 (2020).

[36] S. Ghimire and D. A. Reis, High-harmonic generation from solids, Nat. Phys. **15**, 10 (2019).

[37] E. Goulielmakis and T. Brabec, High harmonic generation in condensed matter, Nat. Photonics **16**, 411 (2022).

[38] J. E. Sipe and A. I. Shkrebtii, Second-order optical response in semiconductors, Phys. Rev. B **61**, 5337 (2000).

[39] F. Willems, C. T. L. Smeenk, N. Zhavoronkov, O. Kornilov, I. Radu, M. Schmidbauer, M. Hanke, C. von Korff Schmising, M. J. J. Vrakking, and S. Eisebitt, Probing ultrafast spin dynamics with high-harmonic magnetic circular dichroism spectroscopy, Phys. Rev. B **92**, 220405(R) (2015).

[40] T. Fan, P. Grychtol, R. Knut, C. Hernández-García, D. D. Hickstein, D. Zusin, C. Gentry, F. J. Dollar, C. A. Mancuso, C. W. Hogle *et al.*, Bright circularly polarized soft X-ray high harmonics for X-ray magnetic circular dichroism, Proc. Natl. Acad. Sci. USA **112**, 14206 (2015).

[41] C. La-O-Vorakiat, M. Siemens, M. M. Murnane, H. C. Kapteyn, S. Mathias, M. Aeschlimann, P. Grychtol, R. Adam, C. M. Schneider, J. M. Shaw *et al.*, Ultrafast demagnetization dynamics at the *M* edges of magnetic elements observed using a tabletop high-harmonic soft X-Ray source, Phys. Rev. Lett. **103**, 257402 (2009).

[42] G. Zhang, M. Si, M. Murakami, Y. Bai, and T. F. George, Generating high-order optical and spin harmonics from ferromagnetic monolayers, Nat. Commun. **9**, 3031 (2018).

[43] D. Xiao, G.-B. Liu, W. Feng, X. Xu, and W. Yao, Coupled spin and valley physics in monolayers of MoS_2 and other group-VI dichalcogenides, Phys. Rev. Lett. **108**, 196802 (2012).

[44] O. Neufeld, D. Ayuso, P. Decleva, M. Y. Ivanov, O. Smirnova, and O. Cohen, Ultrasensitive chiral spectroscopy by dynamical symmetry breaking in high harmonic generation, Phys. Rev. X **9**, 031002 (2019).

[45] R. Yu, H. Weng, Z. Fang, H. Ding, and X. Dai, Determining the chirality of Weyl fermions from circular dichroism spectra in time-dependent angle-resolved photoemission, Phys. Rev. B **93**, 205133 (2016).

[46] Q. Ma, S.-Y. Xu, C.-K. Chan, C.-L. Zhang, G. Chang, Y. Lin, W. Xie, T. Palacios, H. Lin, S. Jia *et al.*, Direct optical detection of Weyl fermion chirality in a topological semimetal, Nat. Phys. **13**, 842 (2017).

[47] F. D. M. Haldane, Model for a quantum Hall effect without landau levels: Condensed-matter realization of the "parity anomaly", Phys. Rev. Lett. **61**, 2015 (1988).

[48] N. Tancogne-Dejean, O. Mücke, F. Kärtner, and A. Rubio, Ellipticity dependence of high-harmonic generation in solids originating from coupled intraband and interband dynamics, Nat. Commun. **8**, 745 (2017).

[49] Y. S. You, D. A. Reis, and S. Ghimire, Anisotropic high-harmonic generation in bulk crystals, Nat. Phys. **13**, 345 (2017).

[50] N. Klemke, N. Tancogne-Dejean, G. M. Rossi, Y. Yang, F. Scheiba, R. Mainz, G. Di Sciacca, A. Rubio, F. Kärtner, and O. Mücke, Polarization-state-resolved high-harmonic spectroscopy of solids, Nat. Commun. **10**, 1319 (2019).

[51] E. Beaurepaire, J.-C. Merle, A. Daunois, and J.-Y. Bigot, Ultrafast spin dynamics in ferromagnetic Nickel, Phys. Rev. Lett. **76**, 4250 (1996).

[52] C. Gong, L. Li, Z. Li, H. Ji, A. Stern, Y. Xia, T. Cao, W. Bao, C. Wang, Y. Wang *et al.*, Discovery of intrinsic ferromagnetism in two-dimensional van der Waals crystals, Nature (London) **546**, 265 (2017).

[53] A. J. Uzan-Narovlansky, L. Faeyrman, G. G. Brown, S. Shames, V. Narovlansky, J. Xiao, T. Arusi-Parpar, O. Kneller, B. D. Bruner, O. Smirnova *et al.*, Observation of interband Berry phase in laser-driven crystals, Nature (London) **626**, 66 (2024).